PHYSICAL REVIEW A VOLUME 27, NUMBER 1 JANUARY 1983

Coherent pump dynamics, propagation, transverse, and diffraction effects in three-level superfluorescence and control of light by light

F. P. Mattar
Aerodynamics Laboratory, Mechanical and Aerospace Engineering Department, Polytechnic Institute of New York, Brooklyn, New York 11201 and Laser Spectroscopy Laboratory, Massachusetts Institute of Technology, Cambridge, Massachusetts 02139

C. M. Bowden
Research Directorate, United States Army Missile Laboratory, United States Army Missile Command, Redstone Arsenal, Alabama 35898

(Received 1 June 1982)

A model is presented for the dynamical evolution of superfluorescence from an optically pumped three-level system. The full propagation, transverse, and diffraction effects are taken into account. With the use of a previously developed algorithm, a computational simulation was constructed from this model and results are presented and discussed. In particular, it is shown that the injected coherent pump-pulse initial characteristics, such as on-axis area, temporal and radial width and shape, can have significant deterministic effects on the superfluorescent pulse delay time, peak intensity, temporal width, and shape. Thus, by specifying certain initial properties of the injected pump pulse, the superfluorescent pulse can be shaped and altered. The results predict the conditions under which an injected light pulse of a given frequency can be used to generate, shape, and control a second light pulse of a different frequency via a nonlinear medium, thus demonstrating a new aspect of the phenomenon of light control by light.

I. INTRODUCTION

Superfluorescence[1] is the phenomenon whereby a collection of atoms or molecules is prepared initially in a state of complete inversion and then allowed to undergo relaxation by collective, spontaneous decay. Since Dicke's initial work,[2] there has been a preponderance of theoretical and experimental work dealing with this process.[3]

With the exception of the more recent work of Bowden and Sung,[4] all theoretical treatments have dealt exclusively with the relaxation process from a prepared states of complete inversion in a two-level manifold of atomic energy levels and thus do not consider the dynamical effects of the pumping process. Yet, all reported experimental work[5–10] has utilized optical pumping on a minimum manifold of three atomic or molecular energy levels by laser pulse injection into the nonlinear medium, which subsequently superfluoresces.

It was pointed out by Bowden and Sung[4] that for a system otherwise satisfying the conditions for superfluorescent (SF) emission, unless the characteristic super-radiance time[1] τ_R is much greater than the pump-pulse temporal duration τ_p, i.e., $\tau_R \gg \tau_p$, the process of coherent optical pumping on a three-level system can have dramatic effects on the SF. This is a condition which has not been realized over the full range of reported data.[3]

In this paper, we present calculational results and analysis for the effects of coherent pump dynamics, propagation, transverse, and diffraction effects on SF emission from an optically pumped three-level system. The full, nonlinear, copropagational aspects of the injected pump pulse, together with the SF which evolves, are explicitly treated in the calculation. Not only do our results relate strongly to previous calculations and experimental results in SF, but we introduce and demonstrate a new concept in nonlinear light-matter interactions, which we call light control by light. We show how characteristics of the SF can be controlled by specifying certain characteristics of the injection pulse in the regime $\tau_p > \tau_R$.

In Sec. II, the model upon which the calculation is based is presented, and the algorithm used in the simulation is outlined. Results of the calculation are presented and discussed in Sec. III. Section IV is used to summarize the results and cite implications and to discuss future work.

II. MODEL FOR THREE-LEVEL SUPERFLUORESCENCE

The model upon which the calculation is based is composed of a collection of identical three-level

atoms, each having the energy-level scheme shown in Fig. 1. The $1\leftrightarrow3$ transition is induced by a coherent electromagnetic field injection pulse of frequency ω_0 nearly tuned to the indicated transition. The properties of this pumping pulse are specified initially in terms of the initial and boundary conditions. The transition $3\leftrightarrow2$ evolves by spontaneous emission at frequency ω. It is assumed that the energy-level spacing is such that $\epsilon_3>\epsilon_2\gg\epsilon_1$ so that the fields at frequencies ω_0 and ω can be treated by separate wave equations. The energy levels $2\leftrightarrow1$ are not coupled radiatively due to parity considerations.

Further, we neglect spontaneous relaxation in the $3\leftrightarrow1$ transition, and spontaneous relaxation in the $3\leftrightarrow2$ transition is simulated by the choice of a small, but nonzero, initial transverse polarization[11] characterized by the parameter $\phi_0\sim10^{-3}$. Our results do not depend upon nominal variations of this parameter. The initial condition is chosen consistent with the particular choice of ϕ_0 (see the Appendix) with nearly all the population in the ground state and the initial values of the other atomic variables chosen consistently[4,12] according to the initial equilibrium properties of the system.[13] The full statistical treatment of the quantum initiation process with resulting temporal fluctuations will be presented in a future development. Thus, the results presented here are to be regarded as expectation values or ensemble averages.

We use the electric-dipole and rotating-wave approximations and couple the atomic dipole moments to classical field amplitudes which are determined from Maxwell's equations. The Hamiltonian which describes the field-matter interaction for this system comprising N atoms[4] is

$$\mathscr{H}=\hbar\sum_{r=1}^{3}\sum_{j=1}^{N}\epsilon_{rj}R_{rr}^{(j)}-\frac{i\hbar}{2}\sum_{j=1}^{N}\{\Omega^{(j)}R_{32}^{(j)}\exp[-i(\omega t-\vec{k}\cdot\vec{r}_j)]-\Omega^{(j)*}R_{23}^{(j)}\exp[i(\omega t-\vec{k}\cdot\vec{r}_j)]\}$$
$$-\frac{i\hbar}{2}\sum_{j=1}^{N}\{\omega_R^{(j)}R_{31}^{(j)}\exp[-i(\omega_0 t-\vec{k}_0\cdot\vec{r}_j)]-\omega_R^{(j)*}R_{13}^{(j)}\exp[i(\omega t-\vec{k}_0\cdot\vec{r}_j)]\}\ . \tag{2.1}$$

The first term on the right-hand side (rhs) of Eq. (2.1) is the free atomic system Hamiltonian with atomic level spacings ϵ_{rj}, $r=1,2,3$; $j=1,2,\ldots,N$. The second term on the rhs describes the interaction of the atomic system with the fluorescence field associated with the $3\leftrightarrow2$ transition, whereas the last term on the right in (2.1) describes the interaction between the atomic system and the coherent pumping field. The fluorescence field and the pumping field have amplitudes $\Omega^{(j)}$ and $\omega_R^{(j)}$, respectively, in terms of Rabi frequency, at the position of the jth atom, $\vec{r}_j$. The respective wave vectors of the two fields are $\vec{k}$ and $\vec{k}_0$, and the carrier frequencies are ω and ω_0. It is assumed that the electromagnetic field amplitudes vary insignificantly over the atomic dimensions and that all of the atoms remain fixed during the time frame of the dynamical evolution of the system.

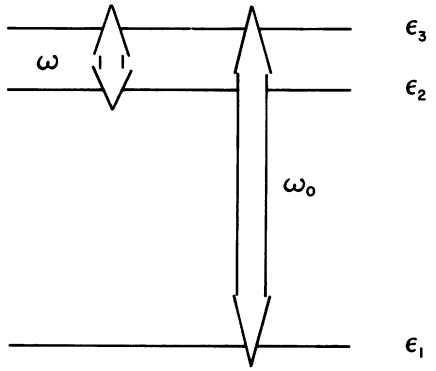

FIG. 1. Model three-level atomic system and electric field tunings under consideration. For the results reported here, the injected pulse is tuned to the $1\leftrightarrow3$ transition.

The atomic variables in (2.1) are the canonical operators[4] $R_{kl}^{(j)}$ which obey the Lie algebra defined by the commutation rules[14–16]

$$[R_{ij}^{(m)},R_{lk}^{(n)}]=R_{ik}^{m}\delta_{lj}\delta_{mn}-R_{lj}^{(m)}\delta_{ik}\delta_{mn}\ , \tag{2.2}$$

where $i,j=1,2,3$; $m,n=1,2,\ldots,N$. The Rabi rates $\Omega^{(j)}$ and $\omega_R^{(j)}$ are given in terms of the electric field amplitudes $E^{(j)}$ and $E_0^{(j)}$, respectively, and the matrix elements of the transition dipole moments $u_{32}^{(j)}$ and $u_{31}^{(j)}$ by

$$\Omega^{(j)}=\frac{E^{(j)}u_{32}^{(j)}}{\hbar}\ , \tag{2.3a}$$

$$\omega_R^{(j)}=\frac{E_0^{(j)}u_{31}^{(j)}}{\hbar}\ , \tag{2.3b}$$

where we have considered only one linear polarization for the two fields and propagation in the positive z direction.

It is convenient to canonically transform (2.1) to remove the rapid time variations at the carrier frequencies ω and ω_0 and the rapid spatial variations due to the wave vectors $\vec{k}$ and $\vec{k}_0$. We assume that the field envelopes $\Omega^{(j)}$ and $\omega_R^{(j)}$ vary much more slowly than the periods ω^{-1} and ω_0^{-1}, respectively. In the transformed representation, we are thus deal-

ing with slowly varying field amplitudes and atomic operators. The desired unitary transformation U, such that

$$\tilde{\mathscr{H}}_T = U\mathscr{H}U^{-1} , \tag{2.4}$$

is given by

$$U(t) = \prod_{j=1}^{N} \exp[i\lambda_a^{(j)}(t)R_{33}^{(j)}] \exp[i\lambda_b^{(j)}(t)R_{22}^{(j)}] , \tag{2.5}$$

where

$$\lambda_a^{(j)}(t) = \omega_0 t - \vec{k}_0 \cdot \vec{r}_j , \tag{2.6a}$$

$$\lambda_b^{(j)}(t) = [(\omega_0 - \omega)t - (\vec{k}_0 - \vec{k}) \cdot \vec{r}_j] . \tag{2.6b}$$

If (2.5) is applied to (2.1) and the commutation rules (2.2) are used, we get for the canonically transformed Hamiltonian $\mathscr{H}_T$,

$$\mathscr{H}_T = \hbar \sum_{j=1}^{N} \Delta^{(j)} R_{33}^{(j)} + \hbar \sum_{j=1}^{N} \delta^{(j)} R_{22} - \frac{i\hbar}{2} \sum_{j=1}^{N} (\Omega^{(j)} R_{32}^{(j)} - \Omega^{*(j)} R_{23}) - \frac{i\hbar}{2} \sum_{j=1}^{N} (\omega_R^{(j)} R_{31}^{(j)} - \omega_R^{*(j)} R_{13}^{(j)}) , \tag{2.7}$$

where

$$\Delta^{(j)} = \epsilon_{33}^{(j)} - \omega_0 , \quad \delta^{(j)} = \epsilon_{22}^{(j)} + \omega - \omega_0 , \quad \epsilon_{11} = 0 . \tag{2.8}$$

The equations of motion for the atomic variables are calculated from (2.7) according to

$$\dot{R}_{kl}^{(j)} = \frac{i}{\hbar} [\mathscr{H}_T, R_{kl}^{(j)}] . \tag{2.9}$$

By imposing the canonical transformation defined by (2.5) we, in fact, transformed to a slowly varying operator representation which is consistent with the slowly varying envelope approximation to be imposed later on in the Maxwell's equations coupled to the hierarchy of first-order equations (2.9).

If (2.7) is used in (2.9), the following hierarchy of coupled nonlinear equations of motion is obtained for the atomic variables:

$$\dot{R}_{33}^{(j)} = -\tfrac{1}{2}(\Omega^{(j)} R_{32}^{(j)} + \Omega^{*(j)} R_{23}^{(j)}) - \tfrac{1}{2}(\omega_R^{(j)} R_{31}^{(j)} + \omega_R^{*(j)} R_{13}^{(j)}) - \gamma_{||}(R_{33}^{(j)} - R_{33}^{(e)}) , \tag{2.10a}$$

$$\dot{R}_{22}^{(j)} = +\tfrac{1}{2}(\Omega^{(j)} R_{32}^{(j)} + \Omega^{*(j)} R_{23}^{(j)}) - \gamma_{||}(R_{22}^{(j)} - R_{22}^{(e)}) , \tag{2.10b}$$

$$\dot{R}_{11}^{(j)} = +\tfrac{1}{2}(\omega_R^{(j)} R_{31}^{(j)} + \omega_R^{*(j)} R_{13}^{(j)}) - \gamma_{||}(R_{11}^{(j)} - R_{11}^{(e)}) , \tag{2.10c}$$

$$\dot{R}_{32}^{(j)} = -i\delta^{(j)} R_{32}^{(j)} - \tfrac{1}{2}\Omega^{*(j)}(R_{22}^{(j)} - R_{33}^{(j)}) - \tfrac{1}{2}\omega_R^{*(j)} R_{12}^{(j)} - \gamma_\perp R_{32}^{(j)} , \tag{2.10d}$$

$$\dot{R}_{12}^{(j)} = -i\delta^{(j)} R_{12} + \tfrac{1}{2}(\Omega^{*(j)} R_{13} + \omega_R^{(j)} R_{32}) - \gamma_\perp R_{12}^{(j)} , \tag{2.10e}$$

$$\dot{R}_{13}^{(j)} = -i\Delta^{(j)} R_{13}^{(j)} - \tfrac{1}{2}\Omega^{(j)} R_{12} + \tfrac{1}{2}\omega_R^{(j)}(R_{33}^{(j)} - R_{11}^{(j)}) - \gamma_\perp R_{13}^{(j)} . \tag{2.10f}$$

In Eqs. (2.10), we have added phenomenological relaxation $\gamma_{||}$ and dephasing $\gamma_\perp$ and taken these to be uniform, i.e., the same parameters for each transition. For the diagonal terms $R_{kk}^{(j)}$ the equilibrium values are designed as $R_{kk}^{(e)}$, the same for all atoms.

We shall treat the Eqs. (2.10) from this point as c-number equations, i.e., expectation values. Further, we assume that all the atoms have identical energy-level structure and also, we drop the atomic labels j, so it is taken implicitly that the atomic and field variables depend upon the spacial coordinates x, y, and z, as well as the time t.

It is convenient to introduce a new set of real variables in terms of the old ones. We let

$$W_{kl} = R_{kk} - R_{ll} , \quad k > l \tag{2.11a}$$

$$R_{kl} = \tfrac{1}{2}(U_{kl} + iV_{kl}) , \quad k > l \tag{2.11b}$$

where U_{kl}, V_{kl}, and W_{kl} are real variables, and $U_{kl} = U_{lk}$, $V_{kl} = V_{lk}$,

$$\Omega = X + iY , \tag{2.11c}$$

$$\omega_R = X_0 + iY_0 , \tag{2.11d}$$

where X, Y, X_0, and Y_0 are real variables.

If the transformation (2.11) is applied to (2.10), the resulting equations of motion for the real variables $\{W_{kl}, U_{kl}, V_{kl}\}$ are

$$\dot{W}_{31} = -\tfrac{1}{2}\{XU_{32} - YV_{32}\} - \{X_0 U_{31} - Y_0 V_{31}\} - \gamma_{||}(W_{31} - W_{31}^{(e)}) , \tag{2.12a}$$

$$\dot{W}_{32} = -\{XU_{32} - YV_{32}\} - \tfrac{1}{2}\{X_0 U_{31} - Y_0 V_{31}\} - \gamma_{||}(W_{32} - W_{32}^{(e)}) , \tag{2.12b}$$

$$\dot{U}_{32}=+\delta V_{32}+XW_{32}-\tfrac{1}{2}(X_0U_{12}-Y_0V_{12}) -\gamma_\perp U_{32}\ , \tag{2.12c}$$

$$\dot{V}_{32}=-\delta U_{32}-YW_{32}+\tfrac{1}{2}(X_0V_{21}+Y_0U_{21}) -\gamma_\perp V_{32}\ , \tag{2.12d}$$

$$\dot{U}_{31}=-\Delta V_{31}-\tfrac{1}{2}(XU_{21}+YV_{21})+X_0W_{31} -\gamma_\perp U_{31}\ , \tag{2.12e}$$

$$\dot{V}_{31}=+\Delta U_{31}-\tfrac{1}{2}(XV_{21}-YU_{21})-Y_0W_{31} -\gamma_\perp V_{31}\ , \tag{2.12f}$$

$$\dot{U}_{21}=-\delta V_{21}+\tfrac{1}{2}(XU_{31}-YV_{31}) +\tfrac{1}{2}(X_0U_{32}-Y_0V_{32})-\gamma_\perp U_{21}\ , \tag{2.12g}$$

$$\dot{V}_{21}=+\delta U_{21}+\tfrac{1}{2}(XV_{31}+YU_{31}) -\tfrac{1}{2}(X_0V_{32}+Y_0U_{32})-\gamma_\perp V_{21}\ . \tag{2.12h}$$

In obtaining Eqs. (2.12), we have made use of the invariant $\mathrm{tr}R=I$

$$I\equiv R_{11}^{(j)}+R_{22}^{(j)}+R_{33}^{(j)}\ . \tag{2.13}$$

It is noted that $\dot{I}=0$ is satisfied identically in (2.10a)–(2.10c) for $\gamma_{||}\to 0$. For $\gamma_{||}\neq 0$, the condition (2.13) together with (2.10a)–(2.10c) constitutes the statement of conservation of atomic density, i.e., particle number.

Equations (2.12) are coupled to Maxwell's equations through the polarizations associated with each transition field. It is easily determined that the Maxwell's equations in dimensionless form in the rotating-wave and slowly varying envelope approximations can be written in the following form:

$$\mathscr{F}_p^{-1}\nabla_\rho^2\begin{bmatrix}-\tilde{X}_0\\ \tilde{Y}_0\end{bmatrix}+\frac{\partial}{\partial\eta_p}\begin{bmatrix}\tilde{Y}_0\\ \tilde{X}_0\end{bmatrix}=d\begin{bmatrix}-U_{31}\\ V_{31}\end{bmatrix}, \tag{2.14a}$$

$$\mathscr{F}_s^{-1}\nabla_\rho^2\begin{bmatrix}-\tilde{X}\\ \tilde{Y}\end{bmatrix}+\frac{\partial}{\partial\eta_s}\begin{bmatrix}\tilde{Y}\\ \tilde{X}\end{bmatrix}=d\begin{bmatrix}-U_{32}\\ V_{32}\end{bmatrix}, \tag{2.14b}$$

where the variables $\tilde{X}$, $\tilde{Y}$, $\tilde{X}_0$, $\tilde{Y}_0$ are the same as those defined in (2.11c) and (2.11d), but in units of $\gamma_\perp$. In the above equations, we have assumed cylindrical symmetry, thus

$$\nabla_\rho^2=\frac{1}{\rho}\frac{\partial}{\partial\rho}\left[\rho\frac{\partial}{\partial\rho}\right].$$

The first term on the left-hand side in (2.14a) and (2.14b) accounts for transverse effects with normalized radial coordinate $\rho=r/r_p$, where r is the radial distance and r_p is a characteristic spatial width. In (2.14), $\eta_{p_s}=zg_{\mathrm{eff},p_s}$, where g_{eff,p_s} is the on-axis effective gain

$$g_{\mathrm{eff},p_s}=\frac{\begin{bmatrix}\omega_0\\ \omega\end{bmatrix}\begin{bmatrix}\mu_{32}\\ \mu_{31}\end{bmatrix}^2 N}{n\hbar c}T_2\ , \tag{2.15}$$

where N is the atomic number density (assumed longitudinally homogeneous), and n is the index of refraction assumed identical for each transition wavelength. The quantity

$$d=\frac{N(r)}{N_0} \tag{2.16}$$

governs the relative radial population density distribution for active atoms. This could have variation, say, for an atomic beam. Equations (2.14) are written in the retarded time τ frame where

$$\tau=t-nz/c\ .$$

From this point on, the dot in Eqs. (2.12) is taken to be $\partial/\partial\tau$. Finally, the first factors on the first terms on the lhs in (2.14) are the reciprocals of the "gain-length" Fresnel numbers defined by

$$\mathscr{F}_{p_s}\equiv\frac{2\pi r_p^2}{\lambda_{p_s}g_{\mathrm{eff}}^{-1}}\ . \tag{2.17}$$

It is seen from (2.14) that for sufficiently large Fresnel number $\mathscr{F}$ the corrections due to transverse effects become negligible. The gain-length Fresnel numbers $\mathscr{F}$ are related to the usual Fresnel numbers $F=2\pi r_p^2/\lambda L$, where L is the length of the medium, by

$$\mathscr{F}/F=g_{\mathrm{eff}}L\ , \tag{2.18}$$

i.e., the total gains of the medium. In the computations, diffraction is explicitly taken into account by the boundary condition that $\rho=\rho_{\max}$ corresponds to completely absorbing walls.

The initial conditions are chosen to establish a small, but nonzero transverse polarization for the $3\leftrightarrow 2$ transition with almost the entire population in the ground state. This requires the specification of two small dimensionless parameters $\epsilon\sim 10^{-3}$ for the ground-state initial population deficit, and $\delta\sim 10^{-3}$ for the tipping angle for the initial transverse polarization for the $3\leftrightarrow 2$ transition. The derivation for the initial values for the various matrix elements is presented in the Appendix, and the results are given by (A22), (A23), and (A28)–(A33).

III. CALCULATION RESULTS AND ANALYSIS

Calculational methods developed earlier[17] and discussed elsewhere[18,19] were applied to the model presented in Sec. II to compute the effects on SF pulse evolution for various initial conditions for the injected (pump) pulse. The results presented here demonstrate many facets of the control and shaping of the SF signal by control of the input signal initial characteristics. The material parameters chosen for these calculations are arbitrary, but correspond roughly to those for optically pumped metal vapors in the regime $\tau_p > \tau_R$.

Thus, although the simulation inherently yields numerically accurate results for particular experimental design, the results reported here must be taken as qualitative. Our main purpose here is to demonstrate and analyze specific correlations between the initial and boundary conditions associated with the injected pump pulse and characteristics of the SF pulse which evolve. In many of the cases which follow, rules are established through the analysis which can be used to predict quantitative results for any particular experimental conditions. Our choice of particular initial and boundary conditions has been motivated in part by processes which may have been operative in experiments which have been reported[5-10] and in part by the feasibility of experimental selection or specification. In connection with the latter, we demonstrate the control of one light signal by another via a nonlinear medium, thus imparting nonlinear information transfer and pulse shaping of the SF from specific initial and boundary conditions associated with the pump injection signal.

Figure 2 shows results of the numerical calculation for the transverse integrated intensity profiles for the copropagating SF and injected pulses at a penetration depth of $z=5.3$ cm in the nonlinear medium. These profiles correspond to what would be observed with a wide aperture, fast, energy detector. The pumping pulses are labeled by capital letters, and the corresponding SF pulses are labeled by the corresponding lower case letters. Each set of curves represents a different initial on-axis area for the pump pulse, i.e., curve A is the reshaped pump pulse at $z=5.3$ cm which had its initial on-axis area specified as $\theta_p=\pi$, and curve a is the resulting SF pulse which has evolved. All other parameters are identical for each set of pulses. The initial conditions for the atomic medium is that nearly all the population is in the ground state ϵ_1 at $\tau=0$, and a small, but nonzero macroscopic polarization exists between levels ϵ_3 and ϵ_2. These two conditions are specified by two parameters ϵ and δ, respectively, and we have chosen $\delta=\epsilon=10^{-3}$ self-consistently as

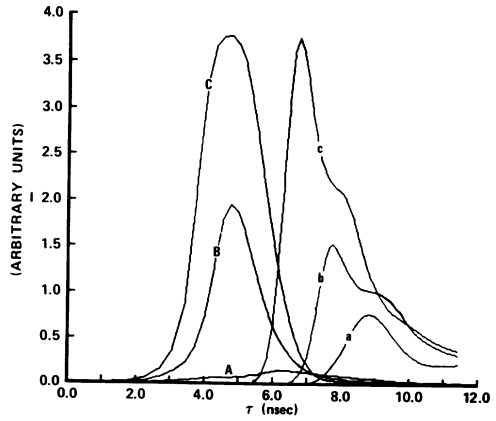

FIG. 2. Radially integrated normalized intensity profiles for the SF and injected pulse at $z=5.3$-cm penetration depth for three different values for the initial on-axis injection pulse area θ_p. The SF pulses are indicated by a, b, and c, whereas the corresponding injected pump pulses are labeled A, B, and C. The injected pulses are initially Gaussian in r and τ with widths (FWHM) $r_0=0.24$ cm and $\tau_p=4$ nsec, respectively. The level spacings are such that $(\epsilon_3-\epsilon_1)/(\epsilon_3-\epsilon_2)=126.6$. The effective gain for the pump transition $g_p=17$ cm^{-1} and that for the SF transition $g_s=291.7$ cm^{-1}. The gain-length Fresnel numbers for the two transitions are $\mathcal{F}_p=16\,800$ and $\mathcal{F}_s=2278$. The relaxation and dephasing times are taken as identical for all transitions and are given as $T_1=80$ nsec and $T_2=70$ nsec, respectively. The injected pulse initial on-axis areas are (A) $\theta_p=\pi$, (B) $\theta_p=2\pi$, and (C) $\theta_p=3\pi$.

specified in the Appendix. These initial conditions are uniform for the atomic medium and are the same for all results reported here. Notice that we have neglected spontaneous relaxation in the pump transition $1\leftrightarrow3$ relative to the SF transition $3\leftrightarrow2$. This is justified owing to our choice of relative oscillator strengths (see Fig. 2 caption).

These results clearly indicate the coherence effect of the initial pump-pulse area on the SF signal which evolves. Notice that the peak intensity of the SF pulses increases monatonically with initial on-axis area for the pump pulse. This is caused by self-focusing due to transverse coupling and propagation. For instance, a 2π-injection pulse would generate a very small SF response compared to an initial π-injection pulse for these conditions at relatively small penetration z, or for the corresponding case in one spatial dimension. Even so, the peak SF intensity is approximately proportional to the square of the pump-pulse initial on-axis area, whereas the delay time τ_D between the pump-pulse peak and the corresponding SF pulse peak is very nearly inversely proportional to the input pulse area. The temporal SF pulse width at full width at half maximum (FWHM) τ_s is approximately invariant with respect

to the injection pulse area.

Since the average values of τ_D and the peak SF intensity are important quantities for interpreting experimental results with theories of SF[1,2,11], the manner in which the pump-pulse coherence and initial on-axis area affects these quantities is seen to be of extreme importance in any analysis.

Figure 3 shows the effect upon the SF pulse of variation in the intitial temporal width at half maximum intensity for the pumping pulse. As the initial temporal width of the injected pulse τ_w becomes smaller, the SF delay time τ_D increases, whereas the peak SF intensity decreases, and the SF temporal width τ_s remains very closely fixed.

It is clear from these results that there exists an approximate linear relationship between the time delay τ_D, between the peak SF intensity and the corresponding pump-pulse intensity, and the initial temporal width τ_p of the pump pulse.

This linear relationship is shown in Fig. 4, where the time delay τ_D is plotted versus the corresponding pump-pulse initial temporal width, from Fig. 3. These results generate the following empirical formula for τ_D as a function of τ_p:

$$\tau_D = 0.375\tau_R[\ln(4\pi/\phi_0)]^2 - 4\tau_R\gamma_\perp(\gamma_R/4\gamma_\perp - 1)\tau_p \ , \tag{3.1}$$

where[20]

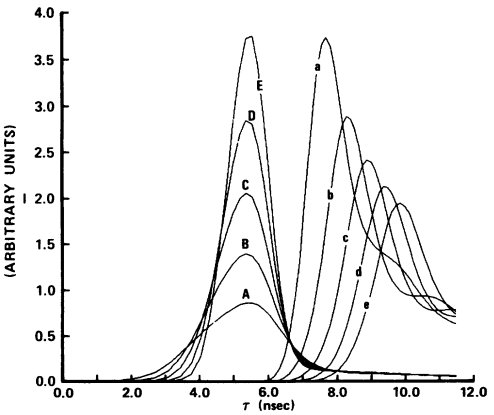

FIG. 3. Radially integrated normalized intensity profiles for the SF and injected pulses at $z=5.3$-cm penetration depth for five different values for the initial temporal width of the injected pulse. The initial on-axis area of the injected pulse is $\theta_p=\pi$, and the pump transition and SF effective gains are $g_p=17.5$ cm^{-1} and $g_s=641.7$ cm^{-1}, respectively. All other parameters except for the Fresnel numbers are the same as those for Fig. 2. The injected pulse initial temporal widths at half maximum are (A) $\tau_p=4$ nsec, (B) $\tau_p=3.3$ nsec, (C) $\tau_p=2.9$ nsec, (D) $\tau_p=2.5$ nsec, and (E) $\tau_p=2.2$ nsec.

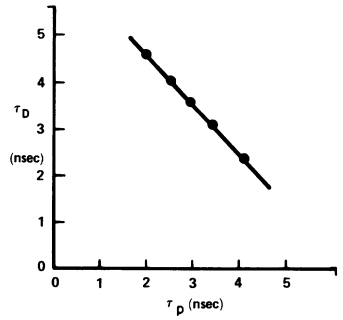

FIG. 4. Delay time τ_D of the SF peak intensity from the corresponding pump-pulse peak intensity vs the pump-pulse initial full temporal width at half maximum intensity τ_p according to Fig. 3.

$$\tau_R = \frac{2T_2}{g_s z} \tag{3.2}$$

is the characteristic superfluorescence time,[1,3] and ϕ_0 is a parameter adjusted to give a best fit to the calculational results. For the case treated here, $\tau_R=41$ psec, $T_2=70$ nsec, and $\phi_0=10^{-8}$, and the Fresnel number $F=1.47$.

The relation (3.1) is at least in qualitative agreement with the analytical prediction made in Ref. 4(b), Eq. (5.1), based upon mean-field theory. The first term in (3.1) was chosen to conform with the quantum-mechanical SF initiation result.[21] The quantity ϕ_0 can be interpreted as the "effective tipping angle" for an equivalent π-initial impulse excitation, i.e., for $\tau_p \to 0$, which initiates subsequent superfluorescence. It is to be noted that the value for ϕ_0 is dependent upon our choice of δ (see the Appendix); however, τ_D varies less than 25% for order-of-magnitude changes in δ for $|\delta| < 10^{-2}$. The choice of δ is simply an artificial way of instigating the semiclassical numerical calculation, and reasonable variations in its value do not strongly affect the results. The physical parameter is, then, ϕ_0, which, interpreted on the basis of (3.1), is generated through the dynamics caused by the pumping process and represents quantum SF initiation. The full statistical treatment for three-level superfluorescence with pump dynamics included will be presented in another publication.[22]

These results emphasize the importance of the initiating pulse characteristics in SF pulse evolution, and the effect of SF pulse narrowing with approximate pulse shape invariance by increasing the initial temporal width of the injected pulse. It is emphasized that all other parameters, including the initial value for the injected pulse on-axis area, are identical among these sets of curves.

The initial radial width r_0 of the injected pulse

was varied and the effect upon the SF pulse evolution is shown in Fig. 5. There is clearly indicated an optimum value for r_0 for which the SF peak intensity is a maximum and the SF temporal width τ_s is a minimum. If the relation (2.18) is used in conjunction with the values of the parameters given in Fig. 5 and its caption, it is seen that optimization occurs for a value for the conventional Fresnel number F_s for the SF transition $F_s \approx 1$. Thus from (2.18) and $F_s = 1$, we have

$$\mathcal{F}_s = g_s z_{\max} \tag{3.3}$$

for the gain-length Fresnel number. Since $F_s \sim 1/z$, the implication is that Eq. (3.3) gives the penetration depth $z_{\max}$ at which the SF peak intensity reaches a maximum in terms of the ratio $\mathcal{F}_s/g_s$. Since this takes both transverse and diffraction explicitly into account as well as propagation, this is indeed a profound statement.

Further insight into the implication of (3.3) can be obtained by considering a one-spacial dimension analogy. If the linear field loss is taken to be entirely due to diffraction, then the one-dimensional linear loss κ corresponding to the two-dimensional case specified by $\mathcal{F}_s$ is given by

$$\kappa_s = \frac{\lambda_s}{2\pi r_0^2} . \tag{3.4}$$

Then, from (2.17),

$$\mathcal{F}_s = \frac{g_s}{\kappa_s} \tag{3.5}$$

is the effective gain g_s to loss κ_s ratio. From the condition (3.3),

$$z_{\max} = (\kappa_s^{-1}) , \tag{3.6}$$

i.e., $z_{\max}$ is the penetration depth at which the SF peak intensity is a maximum and corresponds to one effective diffraction length, as defined by (3.4). Carrying the one-dimensional analogy one step further, (3.5) used in (2.18) gives

$$F = (\kappa z)^{-1} . \tag{3.7}$$

From (3.5) and (3.7) we have exhibited the significance of the Fresnel numbers $\mathcal{F}$ and F in terms of diffraction loss, i.e., $\mathcal{F}$ can be thought of as gain to loss ratio, Eq. (3.5), whereas F can correspondingly be thought of as the reciprocal of the strength of the diffraction loss, Eq. (3.7).

The effect on SF pulse evolution of variation of the initial radial shape of the initiating pulse is shown in Fig. 6. The shape parameter ν is defined in terms of the initial condition for the pump transition field amplitude $\omega_R(r)$:

$$\omega_R(r) = \omega_R(0)\exp[-(r/r_p)^{\nu}] . \tag{3.8}$$

Thus for $\nu = 2$, the initial amplitude of the injected pulse is radially Gaussian, whereas for $\nu = 4$, it is radially super-Gaussian. We see from the results presented in Fig. 6 that as the initial radial shape of the injected pulse becomes broader, i.e., larger values for ν, the peak intensity of the SF pulse generated becomes larger, and the width τ_s and delay time τ_D, diminish. It is emphasized that all other parameters, including the initial values for the radial and temporal widths are invariant among these sets of curves.

Thus if the initial radial shape of the injected pulse is modulated from one injection to the next, the SF temporal width and delay time τ_D are correspondingly modulated as well as the SF peak intensity. Correspondingly, the coherence and initial radial shape of the pump pulse cannot, with validity, be ignored in interpretation of SF experiments in terms of τ_s and τ_D.

Whereas the initial on-axis area for the pumping pulse was $\theta_p = 2\pi$ for the results shown in Fig. 6, the identical conditions and parameters were imposed, but the initial on-axis pump-pulse area was changed

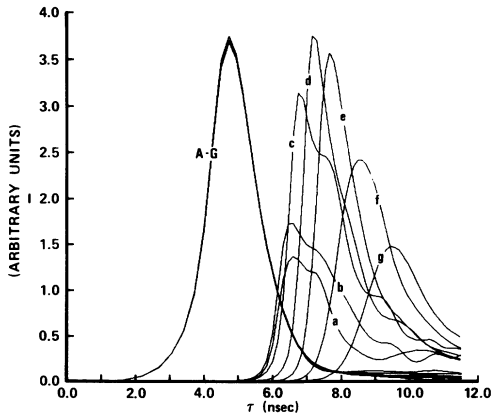

FIG. 5. Radially integrated normalized intensity profiles for the SF and injected pulses at $z = 5.3$-cm penetration depth for seven different values for the injected pulse initial radial width at half maximum r_0. The initial on-axis area θ_p of the injection pulse is $\theta_p = 2\pi$; the SF effective gain $g_s = 758.3$ cm^{-1}, and the pump transition effective gain $g_p = 14.6$ cm^{-1}. All other parameters are the same as for Fig. 2. The initial radial widths at half maximum for the injected pulses are (a) $r_0 = 0.57$ cm, (b) $r_0 = 0.43$ cm, (c) $r_0 = 0.24$ cm, (d) $r_0 = 0.18$ cm, (e) $r_0 = 0.15$ cm, (f) $r_0 = 0.11$ cm, and (g) $r_0 = 0.09$ cm. The corresponding geometrical Fresnel numbers are (a) $F_s = 8.46$, (b) $F_s = 4.79$, (c) $F_s = 1.47$, (d) $F_s = 0.85$, (e) $F_s = 0.57$, (f) $F_s = 0.35$, and (g) $F_s = 0.21$.

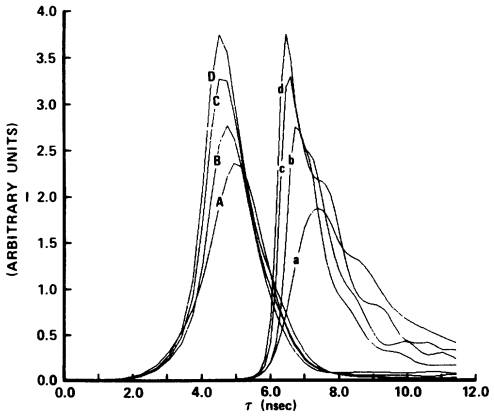

FIG. 6. Radially integrated normalized intensity profiles for the SF and injected pulses at $z=5.3$-cm-penetration depth for four different values for the injected pulse initial radial shape parameter ν (see text). The initial on-axis area θ_p of the injected pulse is $\theta_p=2\pi$, and the SF effective gain $g_s=758.3$ cm^{-1}, whereas the effective gain for the pump transition $g_p=14.6$ cm^{-1}. All other parameters are the same as for Fig. 2. The initial radial shape parameters for the injected pulses are (A) $\nu=1$, (B) $\nu=2$, (C) $\nu=3$, and (D) $\nu=4$.

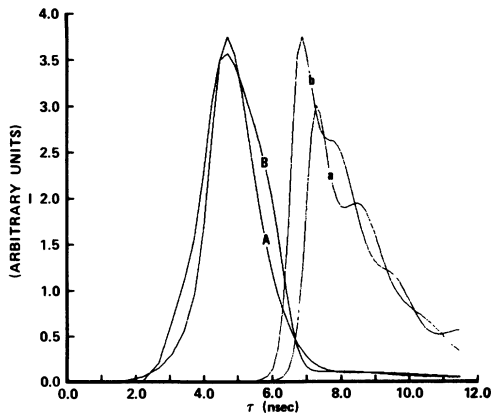

FIG. 8. Radially integrated normalized intensity profiles for the SF and injected pulses at $z=5.3$-cm penetration depth for two different values for the injected pulse initial temporal shape parameter σ (see text). The initial on-axis area θ_p of the injected pulse is $\theta_p=2\pi$, and the SF effective gain $g_s=641.7$ cm^{-1}. All other parameters are the same as for Fig. 5(c). The initial radial shape parameters for the injected pulses are (A) $\sigma=2$ and (B) $\sigma=4$.

to $\theta_p=3\pi$, and the results are shown in Fig. 7. It is seen that the major effect of changing the initial on-axis area from 2π to 3π is to cause more ringing in the SF pulses and to modify the pump-pulse temporal reshaping as is noted by comparing Fig. 7 with Fig. 6.

The response of SF pulse evolution to changes in the initial temporal shape of the injection pulse is shown in Fig. 8, which compares the effect of a Gaussian initial temporal shape for the pump pulse, identified by the temporal shape parameter $\sigma=2$ with that of a super-Gaussian identified by $\sigma=4$. As for the radial distribution discussed previously, the temporal shape parameter σ is defined in terms of the initial condition for the pump transition field amplitude $\omega_R(\tau)$,

$$\omega_R(\tau)=\omega_R(0)\exp[-(\tau/\tau_p)^\sigma] . \tag{3.9}$$

Again, it is seen that the broader initial pump pulse causes an increase in the peak SF intensity and a reduction in the delay time τ_D and SF pulse width τ_s.

Whereas the results of Fig. 8 correspond to an initial on-axis area $\theta_p=2\pi$ for the pump pulse, the results of Fig. 9 correspond to identical conditions and values for the parameters as those for Fig. 8, except that the initial on-axis area for the injection pulse is $\theta_p=3\pi$.

The effect of changing the effective gain for the SF transition g_s and hence the relative oscillator strength between the SF transition and the pump transition is demonstrated in the results of Figs. 10–13. Each of these figures corresponds to a different on-axis initial area θ_p for the injection pulse. Consistent among the entire set of results is that increasing the effective gain g_s results in a nearly linear increase in the SF peak intensity as well as decrease in the delay time τ_D. Also, the smaller area initiating pulse causes a narrower SF pulse to evolve and with apparently less ringing.

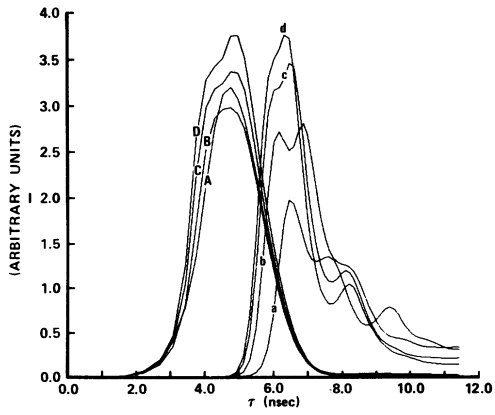

FIG. 7. Radially integrated normalized intensity profiles for the SF and injected pulses at $z=5.3$-cm penetration depth for four different values for the injected pulse initial radial shape parameter ν (see text). The initial on-axis area θ_p of the injected pulse is $\theta_p=3\pi$. All other parameters are the same as for Fig. 6.

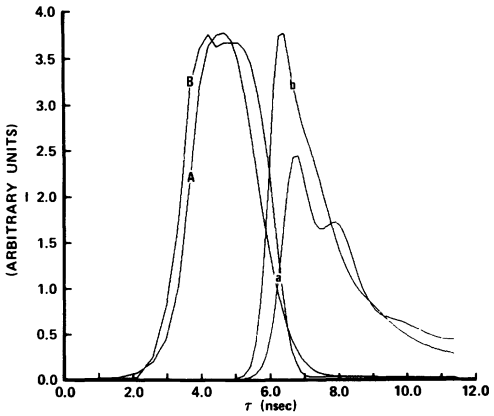

FIG. 9. Radially integrated normalized intensity profiles for the SF and injected pulses at $z=5.3$-cm penetration depth for two different values for the injected pulse initial temporal shape parameter σ (see text). The initial on-axis area θ_p of the injected pulse is $\theta_p=3\pi$. All other parameters are the same as for Fig. 8. The initial radial shape parameters for the injected pulses are (A) $\sigma=2$ and (B) $\sigma=4$.

Figure 14 shows the effect of variation of the density ρ of active atoms. The effective gains g_s and g_p are changed proportionally, corresponding to a density variation ρ. The ratio of the SF intensities is $I_c/I_b=1.76$ and $I_b/I_a=2.06$; these ratios are larger than the corresponding density ratios squared, $(\rho_c/\rho_b)^2=1.40$ and $(\rho_b/\rho_a)^2=1.49$. This difference from the predictions from previous theories of

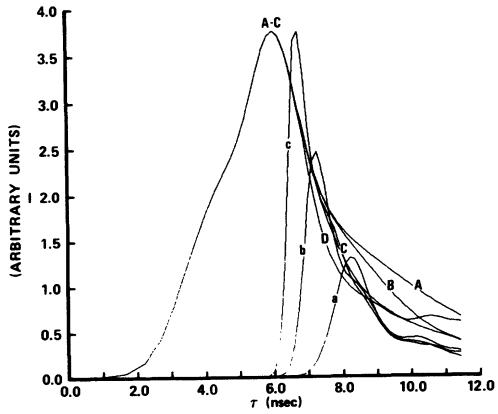

FIG. 10. Radially integrated normalized intensity profiles for the SF and injected pulses at $z=5.3$-cm penetration depth for three different values for the SF transition effective gain g_s. The on-axis initial area θ_p for the injected pulse is $\theta_p=\pi$. All other parameters are the same as those for Fig. 5(c). The SF transition effective gain is (a) $g_s=525.0$ cm^{-1}, (b) $g_s=641.7$ cm^{-1}, and (c) $g_s=758.3$ cm^{-1}.

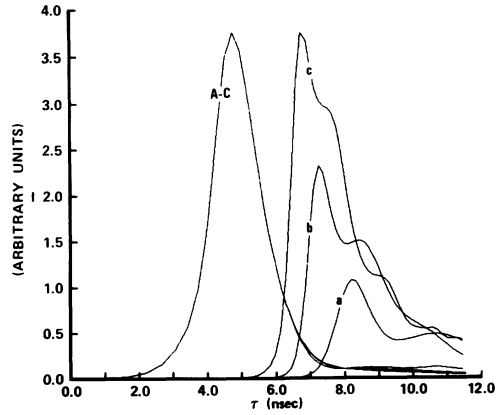

FIG. 11. Radially integrated normalized intensity profiles for the SF and injected pulses at $z=5.3$-cm penetration depth for three different values for the SF transition effective gain g_s. The on-axis initial area θ_p for the injected pulse is $\theta_p=2\pi$. All other parameters are the same as for Fig. 10.

SF[1–3] may be due to self-focusing, especially since the values of the effective gains used in this case are quite high. However, the ratio of the temporal widths τ_s, FWHM, are within 15% of the corresponding inverse ratios of the densities; the same is true for the delay time τ_D of the SF intensity peak with respect to the pump intensity peak. These results compare qualitatively reasonably well with the mean-field predictions for SF in two-level systems initially prepared in a state of complete inversion.[1]

A comparison of the effects upon the injection pulse of variation in oscillator strengths between the

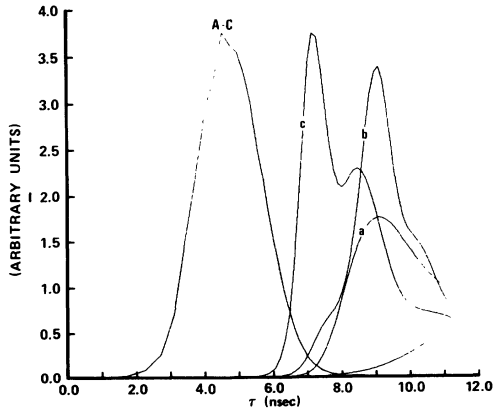

FIG. 12. Radially integrated normalized intensity profiles for the SF and injected pulses at $z=5.3$-cm penetration depth for three different values for the SF transition effective gain g_s. The on-axis initial area θ_p for the injected pulse is $\theta_p=3\pi$. All other parameters are the same as for Fig. 10.

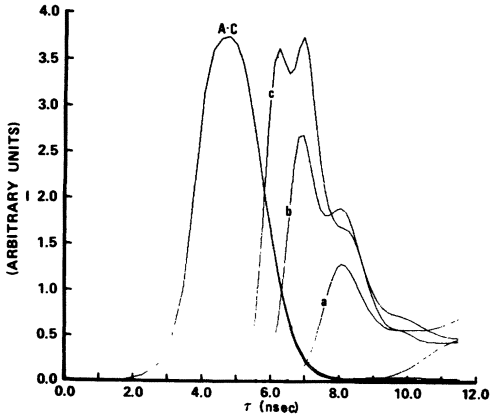

FIG. 13. Radially integrated normalized intensity profiles for the SF and injected pulses at $z=5.3$-cm penetration depth for three different values for the SF transition effective gain g_s. The on-axis initial area θ_p for the injected pulse is $\theta_p=4\pi$. All other parameters are the same as for Fig. 10.

SF and pump transition (variation of g_s) as contrasted to effects upon the pump pulse of a density variation (variation of both g_p and g_s proportionally) is given in Figs. 15 and 16, respectively. It is seen that the respective effects in the pump-pulse reshaping are quite distinct. The variation in oscillator strengths, Fig. 15, essentially causes "hole burning"

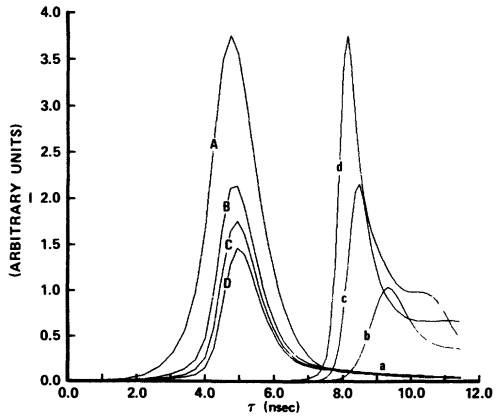

FIG. 14. Radially integrated normalized intensity profiles for the SF and injected pulses at $z=5.3$-cm penetration depth for three different values for the density ρ of atoms. The on-axis initial area θ_p for the injected pulse is $\theta_p=2\pi$. Except for the effective gains and Fresnel numbers, the values for all other parameters are the same as for Fig. 5(c). For each set of curves, the gain values are (b) $g_s=525.0\ \text{cm}^{-1}$, $g_p=26.3\ \text{cm}^{-1}$; (c) $g_s=641.7\ \text{cm}^{-1}$, $g_p=32.1\ \text{cm}^{-1}$; and (d) $g_s=758.3\ \text{cm}^{-1}$, $g_p=37.9\ \text{cm}^{-1}$. The corresponding Fresnel numbers are (b) $\mathcal{F}_p=25\,992$, $\mathcal{F}_s=4100$; (c) $\mathcal{F}_p=31\,724$, $\mathcal{F}_s=5010$; and (d) $\mathcal{F}_p=37\,456$, $\mathcal{F}_s=5922$.

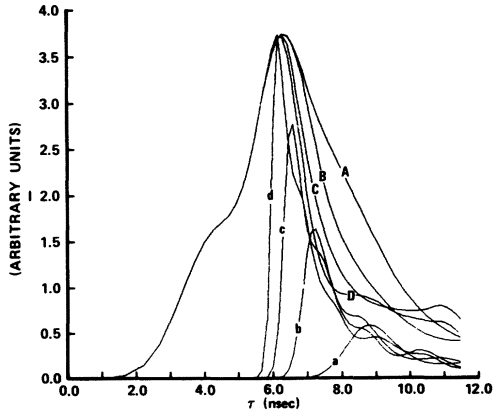

FIG. 15. Radially integrated normalized intensity profiles for the SF and injected pulses at $z=5.3$-cm penetration depth for four different values for the SF transition effective gain g_s. The initial on-axis area for the injected pulse is $\theta_p=\pi$, and the effective gain for the pump transition $g_p=17.5\ \text{cm}^{-1}$. Except for the effective gain g_s, all other parameters are the same as those for Fig. 5(c). The SF transition effective gain g_s for each set of curves is (a) $g_s=291.7\ \text{cm}^{-1}$, (b) $g_s=408.3\ \text{cm}^{-1}$, (c) $g_s=525.0\ \text{cm}^{-1}$, and (d) $g_s=641.7\ \text{cm}^{-1}$.

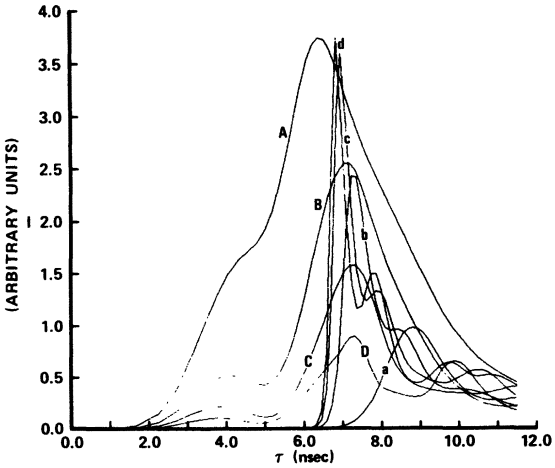

FIG. 16. Radially integrated normalized intensity profiles for the SF and injected pulse at $z=5.3$-cm penetration depth for four different values for the density ρ of atoms. The on-axis initial area θ_p for the injected pulse is $\theta_p=\pi$. Except for the effective gains and Fresnel numbers, the values for all other parameters are the same as for Fig. 5(c). For each set of curves, the gain values are (a) $g_s=291.7\ \text{cm}^{-1}$, $g_p=17.5\ \text{cm}^{-1}$; (b) $g_s=408.3\ \text{cm}^{-1}$, $g_p=24.5\ \text{cm}^{-1}$; (c) $g_s=525.0\ \text{cm}^{-1}$, $g_p=31.5\ \text{cm}^{-1}$; and (d) $g_s=641.7\ \text{cm}^{-1}$, $g_p=38.5\ \text{cm}^{-1}$. The corresponding Fresnel numbers are (a) $\mathcal{F}_p=17\,296$, $\mathcal{F}_s=2278$; (b) $\mathcal{F}_p=24\,212$, $\mathcal{F}_s=3188$; (c) $\mathcal{F}_p=31\,130$, $\mathcal{F}_s=4100$; and (d) $\mathcal{F}_p=38\,048$, $\mathcal{F}_s=5010$.

in the following edge of the pump pulse, whereas the variation in density, Fig. 16, affects the whole pump pulse. This contrast has an analogy as an inhomogeneous, Fig. 15, as opposed to a homogeneous, Fig. 16, effect on the pump pulse. This effect might be used for the purposes of pulse shaping under suitable conditions.

Shown in Fig. 17 is the transverse integrated SF pulse intensity versus retarded time τ (curve 2) together with the transverse integrated pump-pulse intensity versus τ (curve 1) for a gain and propagation depth chosen so that the pulses temporally overlap. Under these conditions the two pulses strongly interact with each other via the nonlinear medium, and the two-photon processes (resonant, coherent Raman—RCR), which transfer populations directly between levels ϵ_2 and ϵ_1, make strong contributions to the mutual pulse development.[4] The importance of the RCR in SF dynamical evolution in an optically pumped three-level system was pointed out for the first time in Ref. 4. Indeed, the SF pulse evolution demonstrated here has greater nonlinearity than SF in a two-level system which has been prepared initially by an impulse excitation. What is remarkable is that this is an example where the SF pulse temporal width τ_s is much less than the pump width τ_p even though the two pulses temporally overlap, i.e., the SF process gets started late and terminates early with respect to the pump time duration. Pulses of this type have been observed[23] in CO_2-pumped CH_3F.

The remaining figures are isometric representations of pump-pulse and SF pulse copropagation and interaction via the nonlinear medium. These figures exhibit details of the dynamic mutual pulse reshaping, self-focusing and defocusing during SF buildup.

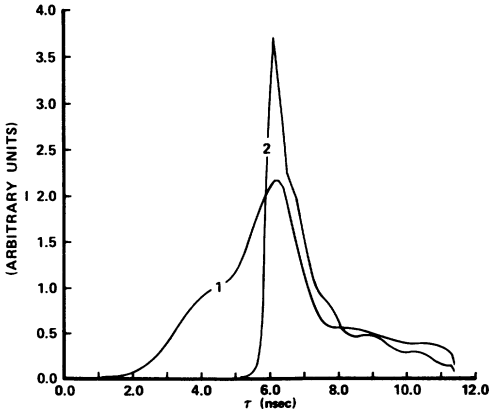

FIG. 17. Radially integrated intensity profiles, in units of Rabi frequency, for the SF (2) and injected pulse (1) at a penetration depth of $z=5.3$ cm. The effective gain for the pump transition and the SF transition are $g_p=17$ cm^{-1} and $g_s=641.7$ cm^{-1}, respectively. The initial on-axis area for the injected pulse is $\theta_p=\pi$. All other parameters are the same as for Fig. 2.

The pulse intensities as functions of the radial coordinate ρ and retarded time τ are presented in Figs. 18 and 19 for two different penetrations $z=4.4$ cm and $z=5.3$ cm, respectively, into the high gain medium. The injected pulse is initially radially and temporally Gaussian. Both the pump pulse and the SF pulse are seen to exhibit considerable self-defocusing with ringing following the main SF peak. At the larger penetration, Fig. 19, a large postpulse appears in both the pump and SF pulse propagation. This is due to energy feedback from the SF to the pump transition. The postpulses overlap, and so the two-photon RCR effects are active and quite significant in the dynamic evolution and coupling between the pump and SF pulses. This effect is due entirely to the coherence in the dynamical evolution of the system.

Portrayed in Figs. 20 and 21 are isometric representations for the radial and temporal dependence of the copropagating injected and SF pulses for two different initial shape distributions for the pump pulse. In the first case, Fig. 20, the initial temporal distribution of the injected pulse is Gaussian, whereas the initial radial distribution is characterized by the parameter $\nu=3$, Eq. (3.8). It is observed that the injected pulse has undergone considerable reshaping, due to propagation, to a more Gaussian radial distribution, and the SF pulse exhibits strong self-defocusing in the wings of the tail region. In the second case, Fig. 21, the initial radial distribution of the injected pulse is Gaussian, whereas the initial temporal distribution is half-Gaussian, with the sharp temporal cutoff on the following temporal half-section of the pulse. The SF pulse rises extremely sharply, in comparison to the other cases analyzed, and tapers off with strong self-defocusing indicated in the wings of the pulse tail. Pump pulses of this type are generated using a plasma switch[10] and the corresponding SF pulses with steep rise have been observed.

IV. CONCLUSIONS

The effects presented here clearly demonstrate the coherence and deterministic effects on SF pulse evolution of injection pump-pulse characteristics and conditions in the regime $\tau_p < \tau_R$. It is suggested that effects of the type discussed here may have in fact been operative in SF experiments and their results which were published earlier.[5–10] The pump pulse was taken as purely coherent in these calculations. To determine whether or not effects of the nature

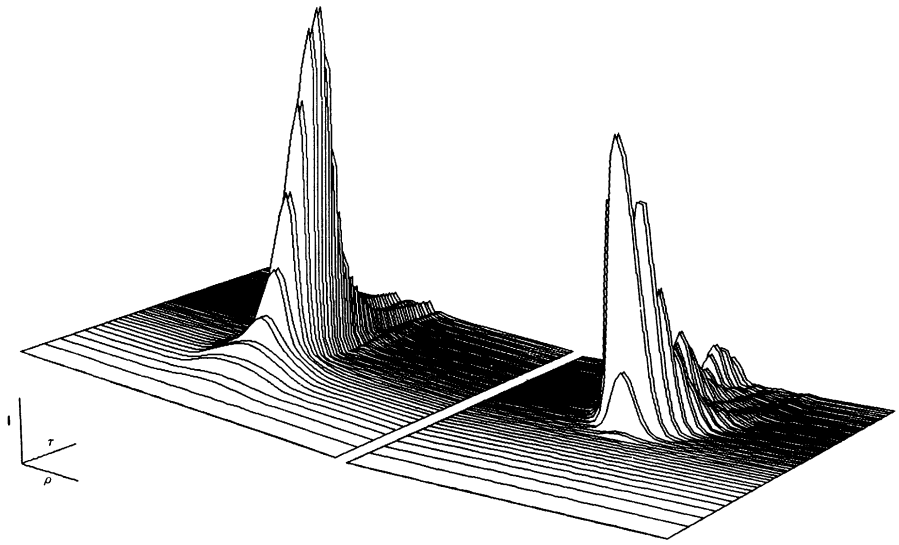

FIG. 18. Pulse intensity I as a function of the radial coordinate ρ and retarded time τ at penetration $z=4.4$ cm. The injected pump pulse is in the upper left, and the SF pulse, which is generated, is in the lower right. The parameters are the same as for Fig. 3(A).

reported here are indeed operative in a given experiment, it is crucial to determine the degree of coherence of the pumping process as well as its temporal duration.[4]

Furthermore, and perhaps of greater importance, we have demonstrated the control and shaping of the SF pulse which evolves by specification of particular initial characteristics and conditions for the pumping pulse which is injected into the nonlinear medium to initiate SF emission. These manifestations and others of the same class we call the control of light by light via a nonlinear medium. This phenomenon constitutes a method for nonlinear information encoding, or information transfer, from

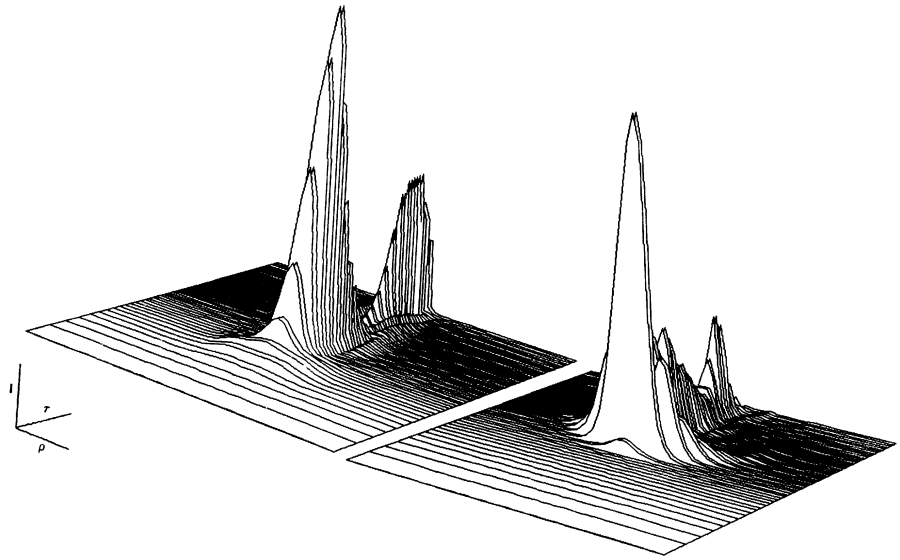

FIG. 19. Pulse intensity I as a function of the radial coordinate ρ and retarded time τ at penetration $z=5.3$ cm. The injected pump pulse is in the upper left, and the SF pulse, which is generated, is in the lower right. The parameters are the same as for Fig. 18.

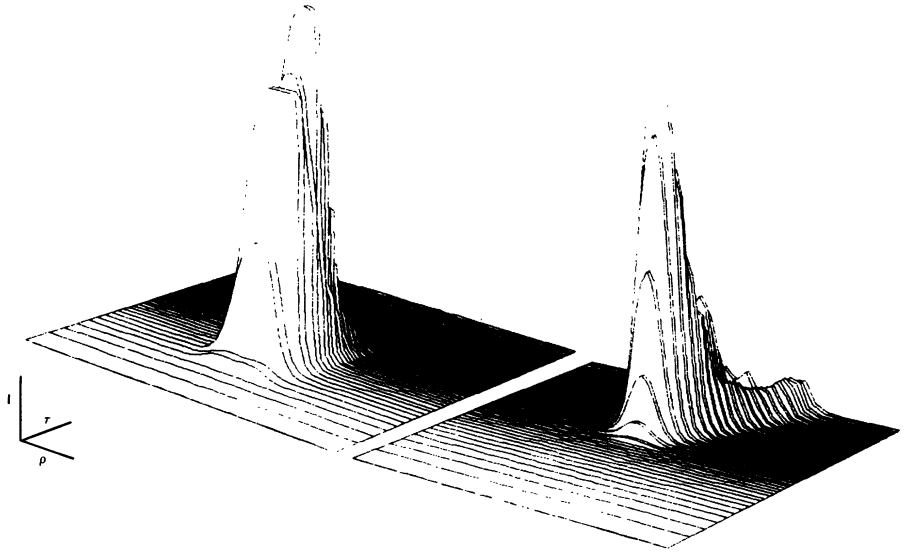

FIG. 20. Pulse intensity I as a function of the radial coordinate ρ and retarded time τ at penetration $z=5.3$ cm. The injected pump pulse is in the upper left, and the SF pulse, which is generated, is in the lower right. The parameters are the same as for Fig. 14(b) except that the initial on-axis area for the injected pump pulse is $\theta_p=3\pi$ and the initial radial shape parameter is $\nu=3$ (see text).

the injection pulse initial characteristics to corresponding SF pulse characteristics which evolve due to propagation and interaction in the nonlinear medium.[22]

Work is now in progress to incorporate the effects of quantum statistics of the SF spontaneous relaxation process.[22] We are in the process of further determination and analysis of the nonlinear interac-

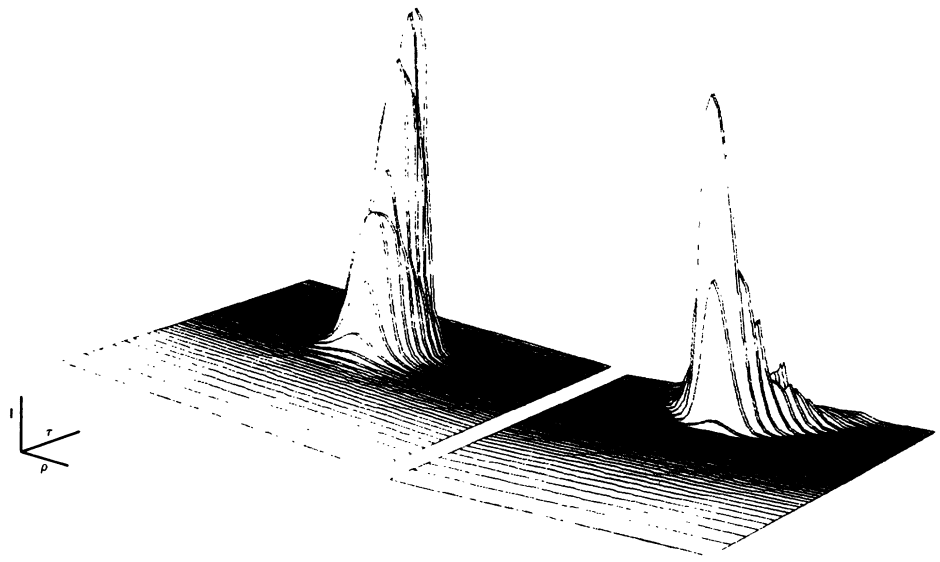

FIG. 21. Pulse intensity I as a function of the radial coordinate ρ and retarded time τ at penetration $z=5.3$ cm. The injected pump pulse is in the upper left, and the SF pulse, which is generated, is in the lower right. The parameters are the same as for Fig. 6(B) except that the initial on-axis area for the injected pulse is $\theta_p=3\pi$, and the initial temporal shape of the injected pulse is half-Gaussian with the sharp temporal cutoff on the following, i.e., increasing τ, side of the pumping pulse.

tion between two copropagating pulses resonantly, as well as nonresonantly, interacting by a nonlinear medium.

ACKNOWLEDGMENTS

The programming assistance of Y. Claude and M. Cormier is gratefully acknowledged. The work of F. P. M. was partially supported by the U. S. Army Research Office, Battelle Columbus Laboratories, and the Office of Naval Research.

APPENDIX

We must choose the initial conditions self-consistently. We wish to establish a small, but nonzero, uniform initial transverse polarization δ for the $3\leftrightarrow 2$ transition. For self-consistency, this corresponds to initial population depletion ϵ of the ground-state population, consistent with (2.13) and Eqs. (2.10).

In terms of initial population numbers N_k,

$$W_{32}=N_3-N_2 \ , \tag{A1}$$

$$W_{31}=N_3-N_1 \ . \tag{A2}$$

We choose

$$N_1=1-\epsilon \ , \tag{A3}$$

ϵ small and positive and impose the ansatz

$$U_{32}=p\sin\delta\sin\phi_s \ , \tag{A4}$$

$$V_{32}=p\sin\delta\cos\phi_s \ , \tag{A5}$$

and let

$$p=\epsilon, \quad N_2/N_3 \ll 1 \ . \tag{A6}$$

The condition (A6) means essentially that $N_3\approx\epsilon$ and $N_2\approx 0$. Equations (A1), (A4), and (A5) under condition (A6) become

$$U_{32}\approx\epsilon\delta\sin\phi_s \ , \tag{A7}$$

$$V_{32}\approx\epsilon\delta\cos\phi_s \ , \tag{A8}$$

$$W_{32}\approx\epsilon\cos\delta \ . \tag{A9}$$

Our uniform initial conditions are just the conditions which led to the linearized mean-field equations in the small fluorescence signal regime of Ref. 4, Eqs. (4.14c)–(4.14f). Initially, the pump field amplitude $\omega_R=0$, and these equations of motion become

$$\dot{R}_{13}=-i\alpha/2A_T R_{12} \ , \tag{A10}$$

$$\dot{R}_{32}=-2i\alpha A_T^{\dagger}R_3 \ , \tag{A11}$$

$$\dot{R}_{12}=-2i\alpha A_T^{\dagger}R_3 \ , \tag{A12}$$

$$\dot{A}_T=-i\alpha R_{23}-\kappa A_T \ , \tag{A13}$$

and A_T is the initial fluorescence field amplitude, $\alpha=g_{\rm eff}\gamma_{\perp}$, and κ is the linear fluorescence field loss. We let

$$R_3\equiv\tfrac{1}{2}W_{32} \ ,$$

and initially,

$$\kappa A_T \gg \frac{\partial A_T}{\partial t} \ . \tag{A14}$$

The condition (A14) in (A13) gives

$$A_T=-\frac{i\alpha}{\kappa}R_{23} \ . \tag{A15}$$

Using (A15) and (A14) to eliminate the field amplitude A_T from Eqs. (A10)–(A13), we get

$$\dot{R}_{31}=-\frac{\alpha^2}{2\kappa}R_{21}R_{32} \ , \tag{A16}$$

$$\dot{R}_{12}=\frac{2\alpha^2}{\kappa}R_{13}R_{32} \ , \tag{A17}$$

$$\dot{R}_{32}=\frac{\alpha^2}{\kappa}W_{32}R_{32} \ . \tag{A18}$$

Dividing (A17) by (A16),

$$\frac{dR_{12}}{dR_{31}}=-4\frac{R_{13}}{R_{21}} \ . \tag{A19}$$

Integrating (A19),

$$R_{13}^2=-\tfrac{1}{4}R_{12}^2 \ , \tag{A20}$$

where the constant of integration has been set equal to zero. Thus

$$R_{13}=\frac{i}{2}R_{12} \ . \tag{A21}$$

In terms of the real variables defined by (2.11b), and using (A21), we get

$$U_{21}=-2V_{32} \ , \tag{A22}$$

$$V_{21}=2U_{32} \ . \tag{A23}$$

From the initial conditions (A1)–(A6),

$$W_{32}\equiv\cos\eta=-1+2\epsilon \ . \tag{A24}$$

Thus

$$\eta=\cos^{-1}(2\epsilon-1) \ , \tag{A25}$$

and

$$U_{31}=\sin\eta\sin\phi_p\approx\eta\sin\phi_p \ , \tag{A26}$$

$$V_{31}=\sin\eta\cos\phi_p\approx\eta\cos\phi_p \ . \tag{A27}$$

We have, therefore, using (A9),

$$W_{32} \approx \epsilon \ , \tag{A28}$$

$$W_{31} = 2\epsilon - 1 \ , \tag{A29}$$

$$U_{32} = \epsilon\delta \sin\phi_s = 0 \ , \tag{A30}$$

$$V_{32} = \epsilon\delta \cos\phi_s = \epsilon\delta \ , \tag{A31}$$

since we must choose the phase ϕ_s such that $\sin\phi_s = 0$. We have

$$U_{31} = \eta \sin\phi_p \ , \tag{A32}$$

$$V_{31} = \eta \cos\phi_p \tag{A33}$$

with η given by (A25) and ϕ_p chosen arbitrarily.

---

[1]R. Bonifacio and L. A. Lugiato, Phys. Rev. A 11, 1507 (1975); 12, 587 (1975).

[2]R. H. Dicke, Phys. Rev. 93, 99 (1954).

[3]See papers and references in *Cooperative Effects in Matter and Radiation,* edited by C. M. Bowden, D. W. Howgate, and H. R. Robl (Plenum, New York, 1977).

[4](a) C. M. Bowden and C. C. Sung, Phys. Rev. A 18, 1558 (1978); (b) 20, 2033 (1979).

[5]N. Skirbanowitz, J. P. Herman, J. C. MacGillivray, and M. S. Feld, Phys. Rev. Lett. 30, 309 (1973).

[6]H. M. Gibbs, Q. H. F. Vrehen, and H. M. J. Hickspoors, Phys. Rev. Lett. 39, 547 (1977).

[7]Q. H. F. Vrehen, Ref. 3, p. 79.

[8]M. Gross, C. Fabre, P. Pillet, and S. Haroche, Phys. Rev. Lett. 36, 1035 (1976).

[9]A. Flusberg, F. Mossberg, and S. R. Hartmann, Ref. 3, p. 37.

[10]A. T. Rosenberger and T. A. DeTemple, Phys. Rev. A 24, 868 (1981).

[11]N. E. Rehler and J. H. Eberly, Phys. Rev. A 3, 1735 (1971).

[12]F. T. Hioe and J. H. Eberly, Phys. Rev. Lett. 47, 838 (1981).

[13]J. R. R. Leite, R. S. Sheffield, M. Duclay, R. D. Sharma, and M. S. Feld, Phys. Rev. A 14, 1151 (1976).

[14]R. Gilmore, *Lie Groups, Lie Algebras, and Some of Their Applications* (Wiley, New York, 1974), Chap. 6, Sec. 2.

[15]R. Gilmore, C. M. Bowden, and L. M. Narducci, Phys. Rev. A 12, 1019 (1975).

[16]R. Gilmore, C. M. Bowden, and L. M. Narducci, in *Quantum Statistics and the Many-Body Problem,* edited by S. B. Trickey, W. R. Kirk and J. W. Dufty (Plenum, New York, 1975).

[17]F. P. Mattar and M. C. Newstein, Ref. 3, p. 139.

[18]F. P. Mattar, in *Optical Bistability,* edited by C. M. Bowden, M. Ciftan, and H. R. Robl (Plenum, New York, 1981), p. 503; in *Proceedings, Tenth Simulation and Modeling Conference, Pittsburgh, 1978,* edited by W. Vogt and M. Mickle (Instrument Society of America, Pittsburgh, 1979).

[19]F. P. Mattar, H. M. Gibbs, S. L. McCall, and M. S. Feld, Phys. Rev. Lett. 46, 1123 (1981).

[20]R. Friedberg and S. R. Hartmann, Phys. Rev. A 13, 495 (1976).

[21]F. Haake, J. Haus, H. King, G. Schroder, and R. Glauber, Phys. Rev. Lett. 45, 558 (1980); D. Polder, M. F. H. Schuurmans, and Q. H. F. Vrehen, Phys. Rev. A 19, 1192 (1979).

[22]C. M. Bowden and F. P. Mattar (unpublished).

[23]T. A. DeTemple (private communication).